UCRL 3747 Rev

# UNIVERSITY OF CALIFORNIA

# Radiation Laboratory

TWO-WEEK LOAN COPY

*This is a Library Circulating Copy which may be borrowed for two weeks. For a personal retention copy, call Tech. Info. Division, Ext. 5545*

BERKELEY, CALIFORNIA

## DISCLAIMER

This document was prepared as an account of work sponsored by the United States Government. While this document is believed to contain correct information, neither the United States Government nor any agency thereof, nor the Regents of the University of California, nor any of their employees, makes any warranty, express or implied, or assumes any legal responsibility for the accuracy, completeness, or usefulness of any information, apparatus, product, or process disclosed, or represents that its use would not infringe privately owned rights. Reference herein to any specific commercial product, process, or service by its trade name, trademark, manufacturer, or otherwise, does not necessarily constitute or imply its endorsement, recommendation, or favoring by the United States Government or any agency thereof, or the Regents of the University of California. The views and opinions of authors expressed herein do not necessarily state or reflect those of the United States Government or any agency thereof or the Regents of the University of California.

UCRL-3747 Rev

UNIVERSITY OF CALIFORNIA
Radiation Laboratory
Berkeley, California

Contract No. W-7405-eng-48

# THE TOTAL CROSS SECTIONS FOR 190-Mev POSITIVELY CHARGED K MESONS IN COMPLEX NUCLEI

Leroy T. Kerth, Thaddeus F. Kycia, and Ludwig van Rossum

September 13, 1957

Printed for the U. S. Atomic Energy Commission

# THE TOTAL CROSS SECTIONS FOR 190-Mev POSITIVELY CHARGED K MESONS IN COMPLEX NUCLEI

Leroy T. Kerth, Thaddeus F. Kycia, and Ludwig van Rossum

Radiation Laboratory
University of California
Berkeley, California

September 13, 1957

## ABSTRACT

The total attenuation cross section and the differential-scattering cross section in one angular interval were measured for $K^+$ mesons of 190-Mev kinetic energy. The targets were carbon, aluminum, copper, silver, and lead.

The cross sections were analyzed in terms of the optical model to determine the parameters of the complex square-well potential. The average real potential was found to be 24.2 ± 2.3 Mev. The mean free path in nuclear matter was determined to be consistent with an average $K^+$-nucleon scattering cross section of about 10 millibarns. Some evidence was found for an increase of the mean free path in nuclear matter with Z.

# THE TOTAL CROSS SECTIONS FOR 190-Mev POSITIVELY CHARGED K MESONS IN COMPLEX NUCLEI*

Leroy T. Kerth, Thaddeus F. Kycia, and Ludwig van Rossum†

Radiation Laboratory
University of California
Berkeley, California

September 13, 1957

## INTRODUCTION

Experiments on the properties of K mesons have indicated an almost complete degeneracy between $K^+$ mesons with various decay modes. Widgoff et al[1] have shown that to a good approximation $K^+$ mesons of different decay modes have the same scattering cross sections. Several measurements of the $K^+$ meson total cross section in nuclear emulsion and the $K^+$ hydrogen cross section have been carried out for energies from 0 to 200 Mev.[2] In this energy range the nuclear potential for $K^+$ mesons was found to be repulsive and of the order of 10 to 20 Mev. In addition, the experiments have shown that the interaction cross section per nucleon in the complex nuclei is smaller than the K hydrogen cross section. The work presented here extends the scattering and interaction cross-section data for 190 Mev $K^+$ mesons to several pure elements.

---

*This work done under auspices of the U. S. Atomic Energy Commission.

†Supported in part by the National Academy of Sciences

## MEASUREMENT OF THE CROSS SECTIONS

The particles emerging from the Bevatron target were momentum-analyzed and focused on the scattering target. Velocity-sensitive counters were used to distinguish between the heavy mesons and the other particles in the beam. Counters placed behind the scattering target indicate the absorption or scatter of a K particle. The nuclei chosen for the measurement were carbon, aluminum, copper, silver, and lead.

### $K^+$ beam

The arrangement of the $K^+$ beam is shown in Fig. 1. The K mesons were produced by the 6.2-Bev protons striking either a carbon or a polyethylene target. (These target materials were chosen with regard to the requirements of an antiproton experiment using the same target.) The particles of momentum 475 Mev/c produced at $0^\circ$ were bent through approximately $45^\circ$ in the magnetic field of the Bevatron, and then left the vacuum through a 0.020-inch-thick dural window. A three-element magnetic-quadrupole strong-focusing lens[3] was placed as close as possible to the window. An analyzing magnet, immediately after the magnetic lens, was used to select the desired momentum.

The quadrupole lens and analyzing magnet together form a "strong-focusing spectrometer."[2, 4] This spectrometer used as objects the virtual images of the target produced by the Bevatron field, and formed a set of real images at the counter array. This experimental arrangement gave a beam of 190-Mev kinetic energy at the scattering target with a spread of $\pm$ 25 Mev and an angular divergence of $\pm 3^\circ$. The flux was 10 K particles per square inch per $10^{10}$ protons incident on the production target.

The function of the counters was threefold: (a) To define the direction of the particles, (b) to select from the momentum-analyzed beam those particles with the proper velocity to have the mass of a K meson, and (c) to determine the fraction of these particles that scattered or interacted in the target. Figure 2 shows the counter array. Angular definition of the particles was provided by two scintillation counters $D_1$ and $D_2$, 1.25 inches in diameter and 0.25 inches thick in the beam direction. These were placed approximately 2 ft apart to define the direction of the incident particles to cone of $3^\circ$ half angle.

Two Cerenkov counters were used to define the velocity of the particles. $C_1$ is a Cerenkov counter using as a radiator Fluoro-chemical 0-75 manufactured by Minnesota Mining and Manufacturing Company. It is a clear liquid with

an index of refraction of 1.276. The photomultiplier tube detects Cerenkov radiation emitted in all directions; thus, the counter is sensitive to all particles with $\beta > 0.784$.

The Cerenkov counter $C_2$, was placed directly behind the first defining counter. It used a radiator of carbon disulphide contained in a glass cylinder with a transparent window at the downstream end. The index of refraction of $CS_2$ is 1.625, so that only particles with $\beta > 0.615$ produce radiation. Light emitted at an angle greater than arcsin (1/n) is internally reflected at the rear window of the counter and does not strike the photomultiplier tube. Thus the counter is insensitive to particles of a velocity greater than $\beta_u$ given by:

$$\beta_u = \frac{1}{n \cos \theta_c}$$

where $\theta_c$ = arcsin (1/n), n = index of refraction. This counter was first described by Fitch.[5] K particles were identified by a coincidence between the $C_2$, $D_1$, and $D_2$ counters in anticoincidence with the $C_1$ counter. When such an event occurred the height of the pulses from the defining counters was recorded and used as a further measure of the velocity.

The scintillation counter P (Fig. 2) was used in conjunction with the absorber to determine, by range, the energy of the incident beam and to check for contamination in the K selection system.

The scattering targets were placed either just behind the P counter or behind the $C_2$ counter. The latter position was used for the "target-out" measurement (which is described more fully below.) The counters $A_1$ and $A_2$ were scintillation counters, 11.5 and 6.75 in. in diameter respectively. The half angles subtended by these counters at the center of the target were $41.3^\circ$ and $22.1^\circ$.

## Electronics and Data Recording

The counters P and $A_2$ used one and four RCA 1P21 photomultipliers respectively. All of the other counters used one RCA 6810 photomultiplier each. The $C_2$ counter and the two defining counters were wired so that a positive signal was available from the last dynode as well as a negative one from the anode. The anode signals from the $C_1$, $C_2$, $D_1$, $D_2$, and P counters were amplified by Hewlett-Packard 460A distributive amplifiers and connected to a six-channel coincidence circuit.[6] This circuit is similar to that described by Garwin.[7] It allows one to mix any combination of the

six inputs into two separate coincidence circuits. An anticoincidence between the outputs of the two circuits is made without destroying either of the two coincidence signals. Because particularly short resolution times were not needed, no attempt was made to obtain maximum resolution of the circuit. Measurements taken during the run indicated a resolving time of about 20 millimicroseconds (mμsec).

The output of the anticoincidence circuit was used to trigger the sweep of a Tektronix 517 Oscilloscope. The dynode pulses from the counters $C_2$, $D_1$, and $D_2$, together with the pulses from the counters $A_1$ and $A_2$ were mixed after suitable delays and displayed on the screen of the oscilloscope. The sweeps were recorded photographically by means of a Du Mont 35-mm moving-film camera. The photographic record allowed pulse-height and timing measurements to be made on each sweep.

The outputs of the coincidence circuits were monitored with Hewlett-Packard prescalers (about 0.1 μsec resolution time for CW) followed by conventional 1-μsec scalers. The anticoincidence circuit was monitored directly with a 1-μsec scaler.

## Pion and Proton Contamination

The composition of the momentum-analyzed beam was approximately 4000 pions, 2000 protons, and 10 K mesons per beam pulse. The $K^+$ attenuation cross sections are a small fraction of the pion or proton cross sections. Therefore, it was necessary for the counters to identify K particles with less than 1% contamination of pions and protons.

The contamination of pions was measured by varying the thickness of the copper absorber in front of the P counter and observing the coincidence rate between the P counter and the K-meson selection system. Because the range of pions is much greater than the range of heavy mesons of the same momentum, we expect the coincidence rate to drop sharply at an absorber thickness equal to the range of the K mesons. From these data (Fig. 3) it was determined that the contamination due to pions was less than 1% of the K flux.

A small contamination resulted from a coincidence between a proton in the defining counters and a random count in the $C_2$ counter. This contamination was discovered from the pulse-height spectra of the two defining counters. By accepting only particles that excited the $C_2$ counter, did not excite the $C_1$ counter, and gave pulse heights in the two defining counters within the proper limits, we selected K particles with less than 1% contamination by other particles.

## Procedure

A target was placed in the K beam directly behind the P counter. Several thousand oscilloscope traces were recorded, and another target was substituted.

The main source of "target-out" attenuation events was the decay in flight of K particles between the P counter and the $A_2$ counter. Using a mean life of $1.3 \times 10^{-8}$ sec,[8] we find that about 6% of the K particles decay between these counters. Because the fraction of particles that interact in the target is about 3%, the background measurement should be as exact as possible. The fraction of the K particles that decay between the P counter and the $A_2$ counter is a function of their velocity. For the "target-out" measurements, the K particles should have the same velocity at corresponding points between the P and $A_2$ counters as for the "target-in" measurement.

For the "target-out" measurement, therefore, the target was placed behind the $C_2$ counter. Thus the particle velocity in the region from the back end of the target to the A counters was the same as for the "target-in" measurement. Only a small correction was then necessary to account for the difference in particle velocity in the region between the P counter and the back of the target. It was sufficient to perform the "target-out" measurement for one target only, because the thickness of the various targets was chosen such that they all would have the same stopping power.

## Reduction of the Data

The pulse height from the two defining counters was calibrated in arbitrary units, using a microfilm reader. This calibration was repeated at various times, to check for any drift in gain of the photomultiplier tubes or amplifiers. It was found that the system was quite stable.

After limits on the proper pulse height for K particles had been determined, a chart was made up showing these limits and the expected position in time of each pulse on the sweep. The timing of a pulse could be read with an accuracy of approximately 5 nanoseconds. Thus the time criteria imposed during the film reading improved the resolving time. Each sweep, as viewed with the microfilm reader was compared with the chart, and the scanner quickly determined from the pulses of the counters $C_2$, $D_1$, and $D_2$ whether or not the event was caused by a K particle. Sweeps due to K mesons were examined for the absence of pulses from the $A_1$ and $A_2$ counters. The sweeps were then classified as one of the following:

X - Events that did not fit the pulse height or time criteria.

$K_0$ - Events that fit the criteria for a K meson but did not have a count in either the $A_1$ or $A_2$ counter.

$K_1$ - Events that fit the criteria and triggered the $A_1$ counter.

$K_2$ - Events that fit the criteria and triggered both the $A_1$ and $A_2$ counters.

F - Events that fit the criteria and triggered only the $A_2$ counter.

The last four of these are of interest. A $K_0$ sweep results from an event giving no charged particle within 41.3° of the beam direction. A $K_1$ event results from a scatter into the angular interval between 22.1° and 41.3°. The $K_2$ events result from particles that scatter less than 22.1° with respect to the beam. The F gives a measure of the accidental rate of the large counters $A_1$ and $A_2$ because an F event can occur only by an accidental coincidence between a K scatter and a random count from the $A_2$ counter.

When a length of film was scanned, the number of events in each class were recorded along with the film number. A total of about 200,000 traces divided into 117 groups was observed. The scanners were not told to which target a particular film corresponded. The data from each group was reduced to a cross section as described in the next section. These cross sections were then compared, and the deviation between them was found to be compatible with the statistical accuracy of each. Thus, it was felt that the scanners were not introducing subjective errors.

## Calculation of the Cross Sections

From the various numbers recorded during the film reading, three cross sections can be calculated; $\sigma_1$ for 22.1° geometry; $\sigma_2$ for 41.3° geometry, and $\Delta\sigma$, the average differential cross section between 22.1° and 41.3°. These cross sections are given by:

$$\sigma_1 = \frac{1}{\eta}\left(\ln \frac{N_0}{N_1} - \ln \frac{N'_0}{N'_1}\right),$$

$$\sigma_2 = \frac{1}{\eta}\left(\ln \frac{N_0}{N_2} - \ln \frac{N'_0}{N'_2}\right), \qquad (1)$$

and

$$\Delta\sigma = \frac{1}{\eta}\left(\ln \frac{N_1}{N_2} - \ln \frac{N'_1}{N'_2}\right),$$

where

$$N_0 = \bar{K}_0 + \bar{K}_1 + \bar{K}_2,$$

$$N_1 = \bar{K}_2,$$

$$N_2 = \bar{K}_1 - \bar{K}_2,$$

$\bar{K}_0$ = number of $K_0$ events in a given run,

$\bar{K}_1$ = number of $K_1$ events in a given run,

$\bar{K}_2$ = number of $K_2$ events in a given run,

primes denote "target-out" data,

and $\eta$ = thickness of the target in atoms/cm$^2$.

The statistical standard deviation on the cross section $\sigma_i$ is equal to

$$\sqrt{\frac{1}{N_0} - \frac{1}{N_i} + \frac{1}{N'_0} - \frac{1}{N'_i}} \; .$$

## CORRECTIONS

### Decay in Flight

The fraction of K particles that decay was greater for the "target-out" case than for the "target-in" case due to the inequality of the velocity between the P counter and the back of the target. The correction was calculated numerically and applied to the data. It accounted for an increase in $\sigma_1$ of 1.6% and for an increase in $\sigma_2$ of 1.9%.

A further correction must be applied to account for $\pi$- and $\mu$-meson contamination arising from $K_{\pi 2}$ and $K_{\mu 2}$ particles that decay between the last defining counter and the target, and trigger the P counter. The fraction of decay products emitted in a direction such as to strike the A counters depends again on the momentum. The secondary particles that do strike the A counters have passed through the target and interacted with cross sections different from that for K particles. These corrections amount to

an increase in $\sigma_1$ and $\sigma_2$ cross sections of 1.8% and 5.5% respectively. The total corrections arising from decay in flight then become 3.4% for $\sigma_1$ and 7.4% for $\sigma_2$.

### Multiple Scattering

The root-mean-square scattering angle for multiple Coulomb scattering for the lead target was $5^{\circ}$. Because the smallest angular resolution used was $22.1^{\circ}$, the contribution from multiple scattering was less than 0.2%.

## CROSS SECTIONS

The measured cross sections are given in the first three rows in Table I. The quantities used in the analysis which follows, are $\sigma/\sigma_g$, where $\sigma_g = \pi R^2$ and R is the radius of the nucleus. R was assumed to be given by $r_0 A^{1/3}$, with $r_0 = 1.41 \times 10^{-13}$ cm. The initial state will be assumed to be represented by a plane wave. A correction to allow for the suppression of the wave at the nucleus by the Coulomb potential can be calculated using the classical expressions for the orbits. The trajectories that just strike the edge of the nucleus of radius R define a cylinder of cross sectional area $\pi b^2$. We find that $b^2 = R^2/(1 + Vc/T)$, where $V_c = (Ze^2)/R$ is the Coulomb potential at the radius R, and T is the kinetic energy of the incident particle. The values of $\pi b^2$ are given in Table I, as well as the cross sections divided by $\pi b^2$.

## COMPLEX SQUARE-WELL ANALYSIS

### Formulation of the Problem

The measured cross sections $\sigma_1$, $\sigma_2$, and $\Delta\sigma$ are actually combinations of the scattering and interaction cross sections. Thus, we can write

$$\sigma_1 = \alpha_1 \sigma_s + \beta_1 \sigma_I,$$

$$\sigma_2 = \alpha_2 \sigma_s + \beta_2 \sigma_I, \qquad (2)$$

and

$$\Delta\sigma = \Delta\alpha \sigma_s + \Delta\beta \sigma_I,$$

where $\sigma_s$ is the total coherent or elastic scattering cross section and $\sigma_I$ is the total incoherent scattering cross section. The latter includes all processes--such as charge exchange and inelastic scattering--that remove particles from the incident plane wave. The $\alpha$'s and $\beta$'s are the fractions of the total elastic and total inelastic-scattering cross sections included in the measurement.

Table I

The measured cross sections from Equation 1 for $K^+$ mesons in the several nuclei (in millibarns) and the values corrected for suppression of the incident wave by the Coulomb field.

| Target | C | Al | Cu | Ag | Pb |
|---|---|---|---|---|---|
| $\sigma_1$ | 96.5 ± 8.5 | 208 ± 13 | 505 ± 28 | 578 ± 38 | 1081 ± 86 |
| $\sigma_2$ | 83 ± 6 | 148 ± 11 | 384 ± 20 | 451 ± 29 | 749 ± 62 |
| $\Delta\sigma$ | 13.0 ± 3.0 | 51 ± 5 | 123 ± 12 | 125 ± 15 | 340 ± 45 |
| $\pi b^2$ | 324 | 543 | 939 | 1320 | 2190 |
| $\frac{\sigma_1}{\pi b^2}$ | 0.298 ± 0.026 | 0.383 ± 0.024 | 0.538 ± 0.030 | 0.438 ± 0.029 | 0.495 ± 0.039 |
| $\frac{\sigma_2}{\pi b^2}$ | 0.256 ± 0.019 | 0.272 ± 0.020 | 0.408 ± 0.021 | 0.342 ± 0.022 | 0.342 ± 0.028 |
| $\frac{\Delta\sigma}{\pi b^2}$ | 0.040 ± 0.009 | 0.094 ± 0.009 | 0.132 ± 0.013 | 0.095 ± 0.012 | 0.155 ± 0.021 |

We now assume that the force between the K meson and the nucleus may be represented by a potential function given by

$$V(r) = V_1 + i\,V_2, \text{ for } r \leq r_0 \tag{3}$$

and

$$V(r) = 0, \qquad \text{for } r > r_0,$$

where $V_1$ and $V_2$ are real and independent of r. Experiments with nuclear emulsion have indicated only constructive interference between the nuclear and the Coulomb-scattering amplitudes.[9] Thus, no attempt was made to fit the data with a negative value of $V_1$.

If we assume that the initial state is given by a plane wave and use the Schroedinger wave equation, the exact phase shifts can be calculated;[10] however, such calculations are quite laborious and are beyond the scope of this paper. The analysis proceeds as follows: The complex potential well is represented by two optical constants, $k_1$ and K, described below. Using the optical model of Fernbach, Serber, and Taylor,[11] we can calculate the numbers $a_1$, $a_2$, $\Delta a$, $\sigma_s$, and $\sigma_I$ of Eq. (2) as functions of $k_1$ and K. The value of $\beta$ can be determined from previous experiments. Values of $k_1$ and K that fit the experimental data are then found.

## Optical Model

The optical model gives approximate solutions valid for small reflection and refraction at the boundary of the potential.

The wave number inside the potential well is given by

$$k' = k_1 + k = k(1 + V_1/E)^{1/2}, \tag{4}$$

where k is the wave number outside the well ($k = P/\hbar$) and $V_1$ is the real part of the potential given in Eq. (3). If we consider the optical analogy to the above problem, $k_1$ corresponds to the real part of the index of refraction. The imaginary part of the interaction is represented by the absorption coefficient K. Fernbach, Serber, and Taylor obtain, for $\sigma_I/\pi R^2$ and $\sigma_s/\pi R^2$

$$\frac{\sigma_I}{\pi R^2} = \{1 - [1 - (1 + 2x)\exp 2x]/2x^2\}, \tag{5}$$

and

$$\frac{\sigma_s}{\pi R^2} = 1 + 1/2\, x^2 \,[1 - (1 + 2x)\exp(-2x)]$$

$$- [1/4\, x^2 + y^2]^{-2} \;\{[1/4\, x^2 - y^2]$$

$$+ \exp(-x)\,[\,2y(1/4\, x^2 + y^2) + xy]\,\sin 2y \qquad (6)$$

$$- \exp(-x)\,[(1/4\, x^2 - y^2) + x(1/4\, x^2 + y^2)]\,\cos 2y\;\},$$

where $x = KR$, $y = k_1 R$.

In addition to Eqs. (5) and (6) the optical model gives, for the scattering amplitude,

$$f(\theta) = \frac{i}{2k} \sum_{\ell = 0}^{\ell m + 1/2 < kR} (2\ell + 1)(1 - e^{(-k + 2ik_1)S_e})\, P_\ell(\cos\theta), \qquad (7)$$

where

$$S_e = [k^2R^2 - (\ell + 1/2)^2]/k.$$

Equation (7) is also obtained by treating the complex square well in WKB approximation.

## The Fractions $a_i$

Using the results of the optical model, we now write

$$a_i = \frac{\int_{\theta_i}^{\pi} [d\sigma(\theta)/d\Omega\,]\,\sin\theta d\theta}{\int_0^{\pi} [d\sigma(\theta)/d\Omega]\,\sin\theta d\theta}\,, \qquad (8)$$

and

$$\Delta a = \frac{\int_{\theta_1}^{\theta_2} [d\sigma(\theta)/d\Omega]\,\sin\theta d\theta}{\int_0^{\pi} [d\sigma(\theta)/d\Omega]\,\sin\theta d\theta}\,, \qquad (9)$$

where $d\sigma(\theta)/d\Omega$ is the differential scattering cross section. Using $d\sigma(\theta)/d\Omega = |f(\theta)|^2$, we calculated $a_i$ and $\Delta a$ and found them to be nearly independent of KR and $k_1R$ and a function of kR only. It has been pointed out that such a conclusion is reasonable, because we expect the shape of

$f(\theta)$ to depend most strongly on the number of partial waves included in the scattering.[12] In the first Born approximation, we find that the shape of $f(\theta)$ is completely independent of $k_1$ and K.

After final values for $k_1$ and K had been obtained, new a's and $\Delta a$'s were calculated and were found to differ from the previous values by less than 1%.

The above analysis is in the framework of Schroedinger wave mechanics, and is therefore not relativistic; however, relativistic kinematics were used.

## Effect of the Coulomb Potential

In the analysis thus far, the Coulomb field has been neglected. If the first Born approximation is used, the scattering amplitude is given by

$$f_c(\theta) = f_c^o(\theta)\, F(\theta), \tag{10}$$

where $f_c^o(\theta)$ is the scattering amplitude derived from a point scatter and $F(\theta)$ is the nuclear form factor. For a uniform charge distribution of radius R, $F(\theta)$ becomes[13]

$$F(\theta) = 4\pi R^3\, [\sin qR - qR \cos qR]/(qR)^3. \tag{11}$$

Equations (10) and (11) give the scattering amplitude as calculated in the Born approximation. It is well known that the magnitude of $f(\theta)$ derived from the Born approximation is nearly exact; however, the phase is not correct. To estimate the maximum effect, the phase of $f_c(\theta)$ was arbitrarily taken to be the same as the phase of $f(\theta)$ given by Eq. (7) for the square well. For all values of K and $k_1$ that were of interest in this problem, the maximum possible Coulomb effect was found to be negligible.

## Values of the fractions $\beta_i$

A K meson that inelastically scatters may still have sufficient energy to reach the A counters, or may give a star prong of sufficient range to count. The fraction of K particles giving rise to such events is $(1-\beta)$. The values of $\beta$ calculated from nuclear emulsion data[14] are

$$\beta_1 = 0.91,$$

$$\beta_2 = 0.81,$$

and

$$\Delta\beta = 0.10. \tag{12}$$

The statistical accuracy of these numbers is about 5% for $\beta_1$ and $\beta_2$, and about 30% for $\Delta\beta$.

Justification for the use of results from nuclear emulsion for the lighter elements is dubious because the value of $\beta$ might well depend on the size of the nucleus. The effect of a variation in $\beta$ on the determination of K and $k_1$ is discussed below.

## Values of the Complex Square - Well Parameters

From Eqs. (2), (5), and (6), and the values of $\alpha$ and $\beta$, one can determine K and $k_1$ pairs that fit each measured cross section. Thus, for each target, one may construct three curves that give the values of K and $k_1$ appropriate to each of the measured cross sections. Figure 4 gives a typical set of these curves. The dotted lines indicate the uncertainty in the various curves because of the statistical errors on the measured cross sections. As is expected, $\sigma_1$ and $\sigma_2$ are nearly independent of $k_1$, whereas $\Delta\sigma$ depends on both K and $k_1$.

The values of K and $k_1$ for each target as determined from the intersection of these curves are given in Table II.

Table II

Values of $k_1$ and K derived from the measured cross section (in units of $10^{13}$ $cm^{-1}$)

| | C | Al | Cu | Ag | Pb |
|---|---|---|---|---|---|
| $-k_1$ | 0.078 ± 0.062 | 0.191 ± 0.029 | 0.240 ± 0.050 | 0.146 ± 0.030 | 0.185 ± 0.046 |
| K | 0.087 ± 0.003 | 0.077 ± 0.012 | 0.077 ± 0.009 | 0.060 ± 0.008 | 0.058 ± 0.009 |

The errors shown reflect only the statistical inaccuracy in the measured cross sections. The systematic errors of the analysis may be larger. The uncertainty of extending to lower Z the value of $\beta$ determined for nuclear emulsion has practically no effect on K; however it certainly affects $k_1$. The values of $k_1$ in Table II should be reliable to about±50%. The values of K must be taken in the spirit of the square-well approximation and considered as only a first approximation to the real physical potential.

From the values of $k_1$ given in Table II the real potential can be calculated from Eq. (4) (Fig. 5). The average potential is found to be 24.2 ± 2.3 Mev.

## Mean Free Path for Interaction in Nuclear Matter

The problem of deriving the cross section for individual K-nucleon interactions from the mean free path in nuclear matter is a difficult one. In the simplest picture, one assumes that each nucleon within the nucleus can interact with the K particle independently of the other nucleons. Thus, we may express the mean free path within the nucleus as:

$$\lambda = K^{-1} = (\sigma_0 \rho)^{-1} \tag{13}$$

where K is the absorption constant as before, $\sigma_0$ is the K-nucleon cross section, and $\rho$ is the nuclear density. For $R = r_0 A^{1/3}$, $\rho$ is given by

$$\rho = \frac{3}{4} (\pi r_0^3)^{-1}. \tag{14}$$

The values of $\sigma_0$ were computed from Eq. (13) and (14) for the values of K given in Table II.

Sternheimer has pointed out that the cross section in complex nuclei is suppressed because of the Pauli exclusion principle operating between identical nucleons in the nucleus.[15] If we assume a Fermi energy of 25 Mev, the average free K-nucleon cross section $\sigma_f$ is given by $\sigma_0/0.884$. The dotted points in Fig. 6 show $\sigma_f$ as derived from the values of $\sigma_0$, computed above.

# DISCUSSION

## Real Potential

The real potentials shown in Fig. 5 may be compared with results from experiments with nuclear emulsion[9,16] for $K^+$ mesons of lower energy. The values at low energy are about 10 to 15 Mev. Thus the values here are significantly larger, indicating an increase of the real potential with increasing K energy. The results here are in reasonable agreement with preliminary nuclear emulsion results at similar energies.[14]

## Absorption Constant

The average cross section per nucleon in complex nuclei from Fig. 6 is lower than the K-proton cross section given by other experiments. The decrease in $\sigma_f$ with increasing A is too large to be explained by the neutron excess even if the K-neutron cross section is as small as one-half the K-proton cross section (as small as is allowed by the conservation of isotopic spin). A failure of the simple model used for the nucleus may account for the decrease. Calculations using a more realistic nuclear density distribution will be carried out in the future.

## ACKNOWLEDGMENTS

The experiment would have been impossible without the assistance, freely contributed during the actual run, of Dr. Robert Birge, Dr. Marian Whitehead, Dr. Robert Lanou, Dr. Jack Sandweiss, Dr. Roy Haddock, Mr. Robert L. Fry, Jr., and Mr. Thomas T. Reynolds. The help of Mr. Robert Fry, Mr. Thomas Reynolds, Mrs. Marilynn Harbert, and Miss Betty Blaine in scanning the film is greatly appreciated. Dr. Donald Stork is thanked for valuable discussions during the initial stages of the experiment, and for the method of analysis taken from his doctoral dissertation. Dr. Jack Sandweiss contributed many suggestions during the analysis.

We also thank Dr. Edward J. Lofgren and the operating crew of the Bevatron for efficient and effective operation of the machine.

## References


1. Widgoff, Shapiro, Schluter, Ritson, Pevsner, and Henri, Phys. Rev. 104, 811 (1956).
2. See for instance, Pisa Conference Report; Nuovo Cimento Suplemento, Vol. IV, No. 2 (1956).
3. Courant, Livingston, and Snyder, Phys. Rev. 88, 1190 (1952).
4. Kerth, Stork, Birge, Haddock, and Whitehead, Bull. Am. Phys. Soc. 30, No. 3, 41 (1955).
5. V. Fitch and R. Motley, Phys. Rev. 101, 496 (1956).
6. Radiation Laboratory Counting Handbook, UCRL-3307, Jan. 1956.
7. Richard L. Garwin, Rev. Sci. Instr. 24, 618 (1953).
8. Alvarez, Crawford, Good, and Stevenson, in Proceedings of the Sixth Annual Rochester Conference on High-Energy Physics, 1956 (Interscience, New York, 1956).
9. D. Fournet Davis, Univ. of Rochester, (to be published); Joseph E. Lannutti, University of Florida (private communication).
10. Leonard I. Schiff, Quantum Mechanics (McGraw-Hill, New York, 1949).
11. N. C. Francis and K. M. Watson, Am. J. Phys. 21, 659 (1953); Fernbach, Serber, and Taylor, Phys. Rev. 75, 1352 (1949).
12. Donald H. Stork, Phys. Rev. 93, 868 (1954).
13. Leonard T. Schiff, Phys. Rev. 92, 988 (1953) and M. E. Rose, Phys. Rev. 73, 279 (1948).
14. Joseph E. Lannutti (private communication).
15. R. M. Sternheimer, Phys. Rev. 106, 1027 (1957).
16. Donald H. Perkins, H. H. Wills, Physical Laboratory, University of Bristol, Bristol, England, (private communication).

## Figure titles

Fig. 1. The $K^+$ beam. Particles leaving the production target parallel to the incident beam were bent by the magnetic field of the Bevatron, focused, and then analyzed to improve the momentum selection. The heavy concrete shielding that surrounded the entire apparatus is not shown.

Fig. 2. Counter array. Counters $D_1$ and $D_2$ define the beam size and direction. $C_1$ is a Cerenkov counter that counts particles of $\beta > 0.77$ and is used in anticoincidence to eliminate $\pi$ mesons. $C_2$ is also a Cerenkov counter that detects particles of $0.62 < \beta < 0.78$ and thus counts K mesons. P and $A_2$ are scintillation counters. Only the sensitive region of the counters is shown.

Fig. 3. Counting rate vs absorber thickness in $g/cm^2$. The mean momentum when the stopping power of the counters is included is 555 Mev/c incident on the first counter.

Fig. 4. Determination of K and $k_1$ for aluminum.

Fig. 5. Experimental values of the real potential $V_1$. Statistical errors are shown.

Fig. 6. The average cross section per nucleon for the various nuclei. These were calculated using the experimental cross sections and assuming the independent particle model. The values have been corrected for the effect of the Pauli exclusion principle.

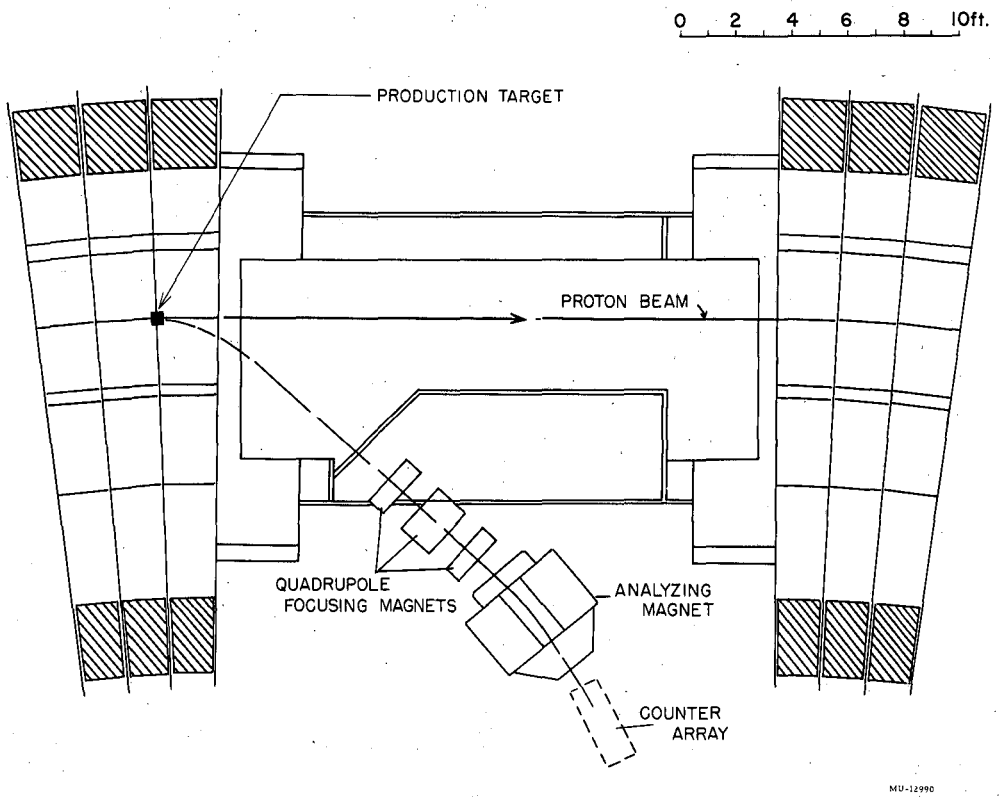
0 2 4 6 8 10ft.
PRODUCTION TARGET
PROTON BEAM
QUADRUPOLE
FOCUSING MAGNETS
ANALYZING
MAGNET
COUNTER
ARRAY
MU-12990

Fig. 1

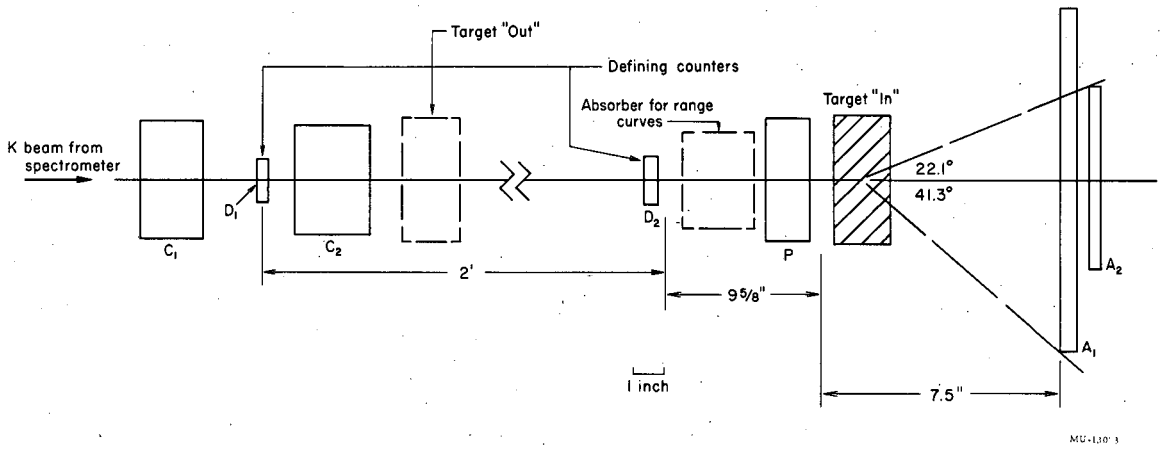
Target "Out"
Defining counters
Absorber for range curves
Target "In"
K beam from spectrometer
22.1°
41.3°
$D_1$
$C_1$
$C_2$
$D_2$
P
$A_2$
$A_1$
2'
9⅝"
1 inch
7.5"

Fig. 2

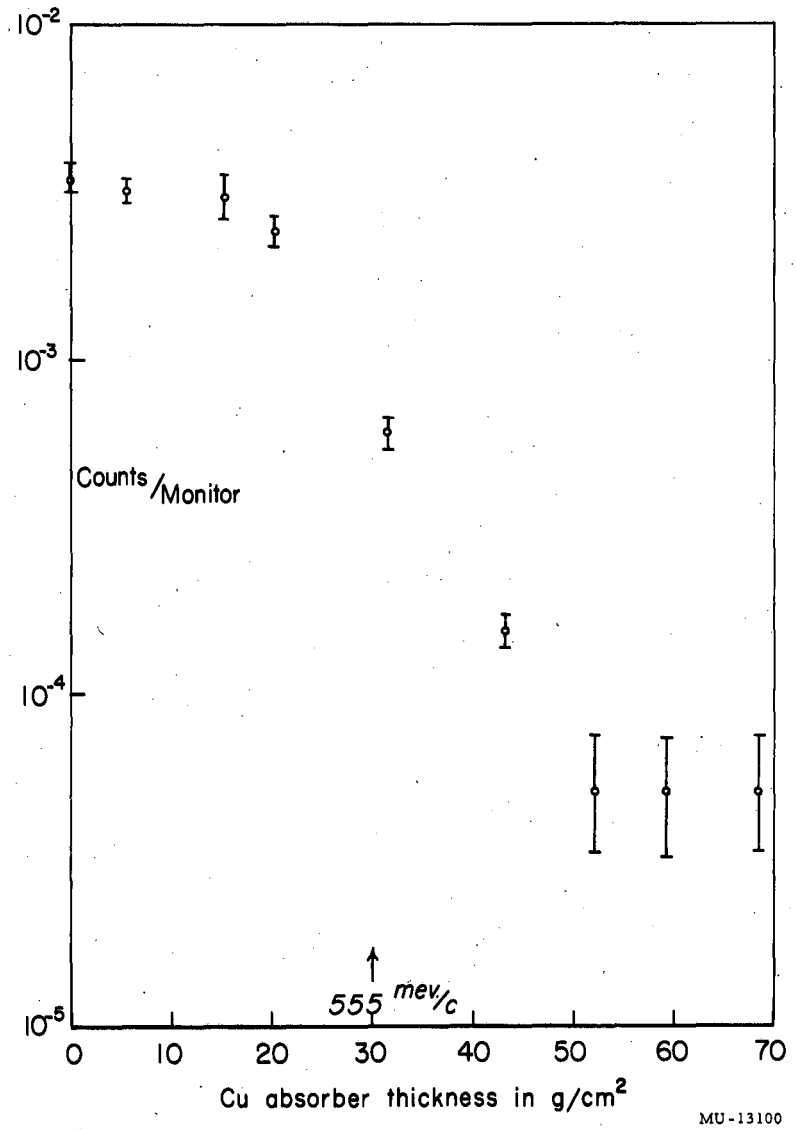
$10^{-2}$
$10^{-3}$
$10^{-4}$
$10^{-5}$
Counts/Monitor
555 mev/c
0
10
20
30
40
50
60
70
Cu absorber thickness in g/cm$^2$
MU-13100

Fig. 3

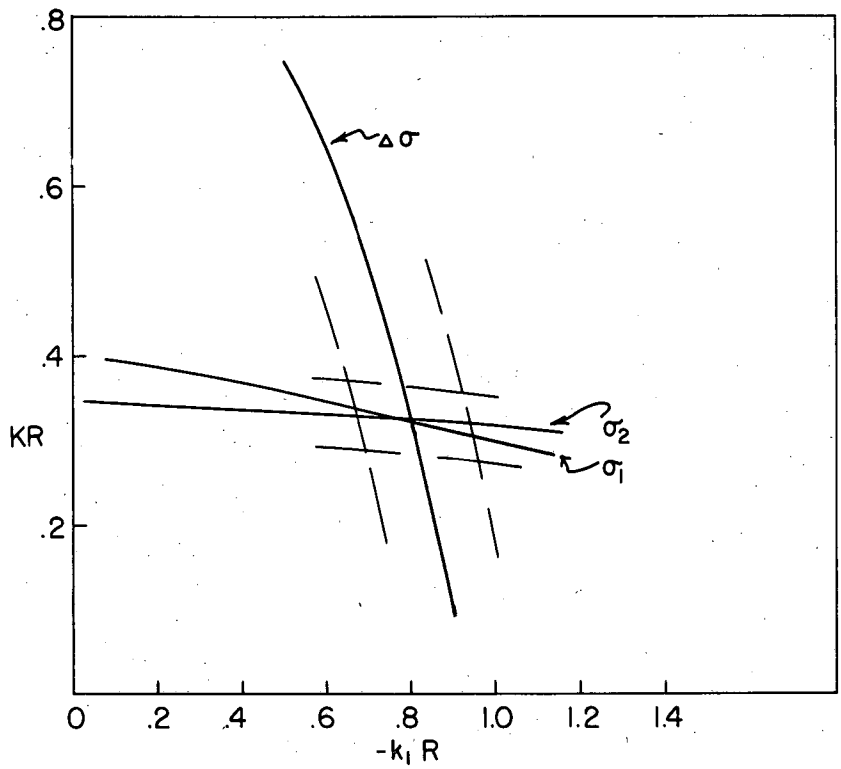


MU-13008

Fig. 4

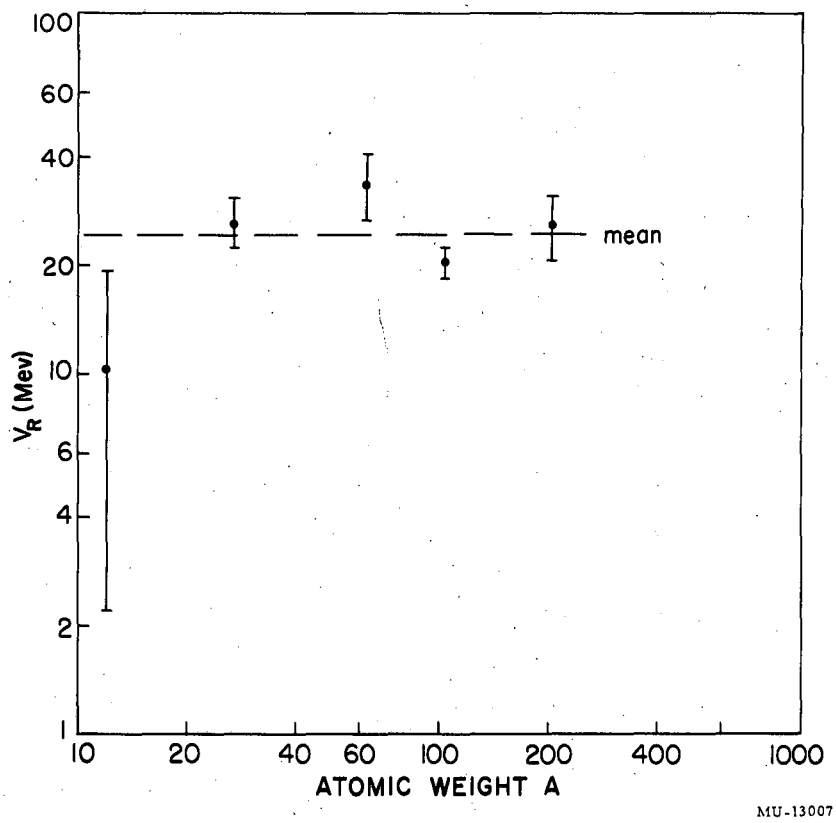
100
60
40
20
10
6
4
2
1
$V_R$ (Mev)
mean
10
20
40
60
100
200
400
1000
ATOMIC WEIGHT A
MU-13007

Fig. 5

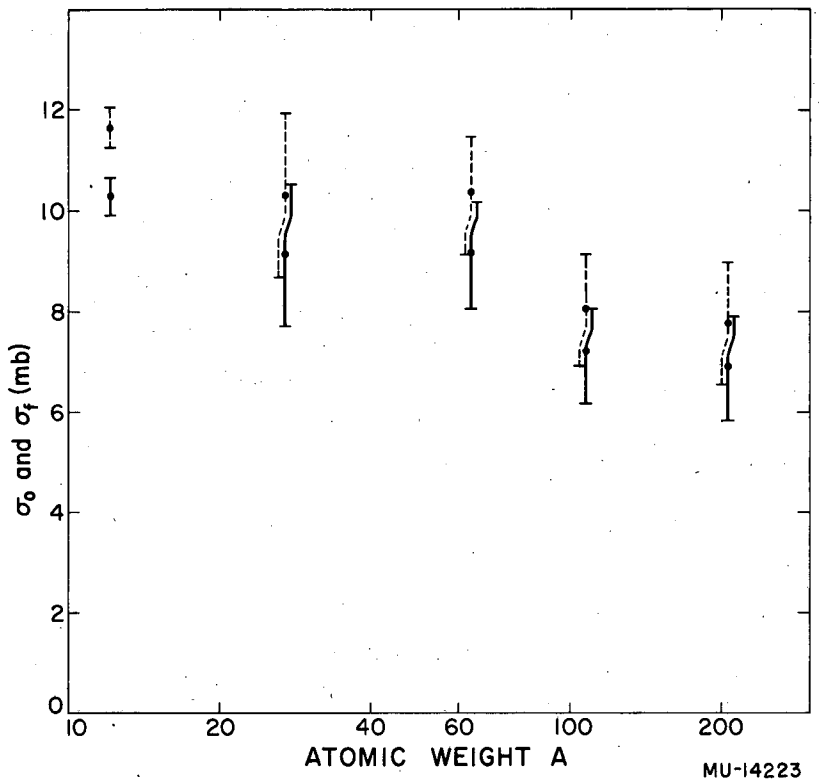
12
10
8
6
4
2
0
$\sigma_o$ and $\sigma_f$ (mb)
10
20
40
60
100
200
ATOMIC WEIGHT A
MU-14223

Fig. 6